nature electronics

ARTICLES

https://doi.org/10.1038/s41928-020-0399-7

Robust and efficient wireless power transfer using a switch-mode implementation of a nonlinear parity–time symmetric circuit

Sid Assawaworrarit and Shanhui Fan ✉

Stationary wireless power transfer has been deployed commercially and can be used to charge a variety of devices, including mobile phones and parked electric vehicles. However, wireless power transfer set-ups typically suffer from an inherent sensitivity to the relative movement of the device with respect to the power source. Nonlinear parity–time symmetric circuits could be used to deliver robust wireless power transfer even while a device is moving rapidly, but previous implementations have relied on an inefficient gain element based on an operation-amplifier circuit, which has inherent loss, and hence have exhibited poor total system efficiency. Here we show that robust and efficient wireless power transfer can be achieved by using a power-efficient switch-mode amplifier with current-sensing feedback in a parity–time symmetric circuit. In this circuit, the parity–time symmetry guarantees that the effective load impedance on the switch-mode amplifier remains constant, and hence the amplifier maintains high efficiency despite variation of the transfer distance. We experimentally demonstrate a nonlinear parity–time symmetric radiofrequency circuit that can wirelessly transfer around 10 W of power to a moving device with a nearly constant total efficiency of 92% and over a distance from 0 to 65 cm.

Wireless power transfer is increasingly used in a range of practical applications[1–18]. A standard wireless power transfer system consists of two magnetically coupled resonators, one on the source side and one on the receiver side. Efficient power transfer is established by carefully adjusting the system parameters, including the rates at which energy is injected into and drawn out of each resonator, as well as the frequency at which the source resonator is driven[1,2,12–14]. Because the optimal values of these parameters often depend sensitively on the coupling strength between the source and receiver resonators, in the standard wireless power transfer system it remains a challenge to robustly deliver wireless power at high power efficiency to a receiver that moves relative to the source over a range of transfer distances.

To harness the full benefits of wireless power delivery, it is important to develop an efficient and robust scheme that is capable of power delivery to a moving device[19]. Recent work[3,5–7] has shown that the parity–time (PT) symmetry concept can be used to enable robust dynamic wireless power transfer. The study of PT symmetry[20,21] in wave systems with carefully designed gain and loss profiles has led to the discovery of a number of intriguing effects such as intrinsically single-mode lasing[22], loss-induced transmission[23], unidirectional reflectivity[24] and chiral dynamics[25], as well as promising applications such as ultrasensitive sensors[26–28].

We previously proposed the use of a nonlinear PT-symmetric circuit to enhance the robustness of wireless power transfer schemes[3]. This scheme, which we refer to here as a PT-symmetric wireless power transfer scheme, consists of a source resonator with saturable gain coupled to a lossy receiver resonator with a load that consumes power (Fig. 1a; an equivalent circuit representation is shown in Fig. 1b, where the loading effect of the receiver is modelled with an equivalent impedance $Z_{eq}(\omega,k)$ that depends on the frequency and the coupling constant k). In contrast to standard wireless power transfer schemes, where the power is injected into the source resonator by a radiofrequency source at a fixed frequency, here the power is instead injected through the gain element incorporated into the source resonator. This PT-symmetric set-up automatically oscillates at a frequency that is optimal for wireless power transfer and hence can achieve constant transfer efficiency and deliver a consistent power level for a wide range of transfer distances, without any need for external tuning. Related work on using gain to achieve self-oscillation in wireless power transfer circuits has also been reported by others[5].

With our approach, we previously achieved a transfer efficiency value exceeding 90% for dynamic wireless power transfer[3]. However, the system efficiency was only ~10%, due mostly to the low energy-injection efficiency of the operational-amplifier circuit that was used as the gain element. It is known that switch-mode amplifiers can provide much higher energy-injection efficiency, and there have been efforts to incorporate switch-mode amplifiers into PT-symmetric wireless power transfer systems[6,7]. In this Article, we elucidate the physical mechanism that governs the efficient operation of a switch-mode amplifier in PT-symmetric wireless power transfer circuits, and show that the PT symmetry can guarantee a constant effective load impedance on the switch-mode amplifier, even with variation of the transfer distance. We develop a circuit design that uses a switch-mode amplifier and current-sensing phase-delay feedback. With this approach, a robust wireless power transfer can be achieved with a total system efficiency of over 90% in the strong coupling region.

Underlying concepts of PT-symmetric wireless power transfer

In a PT-symmetric wireless power transfer scheme, power flow starts at the gain element embedded inside the source resonator, which receives supplied power and continually injects power into the source resonator. The coupling between the two resonators provides a power transfer path from the source to the receiver, where power is delivered to the load. The time evolution of the amplitudes

Department of Electrical Engineering, Ginzton Laboratory, Stanford University, Stanford, CA, USA. ✉e-mail: shanhui@stanford.edu

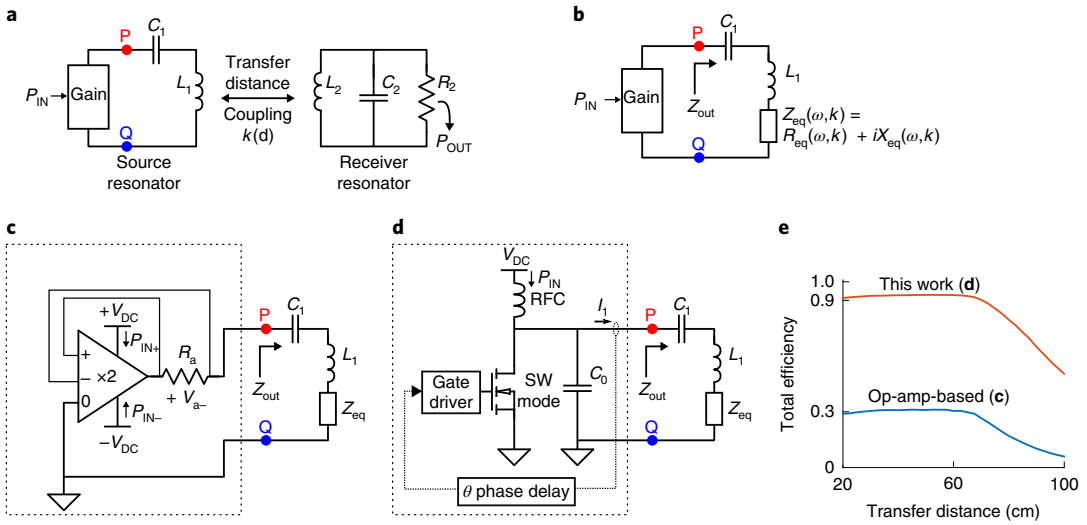

Fig. 1 | Circuit design for efficient and robust wireless power transfer based on nonlinear PT symmetry. a,**b**, Schematics of a PT-symmetric wireless power transfer system shown with separate source and receiver resonators (**a**) and with an equivalent load model (**b**). **c**, Circuit diagram with an operational-amplifier-based gain design[3]. **d**, Circuit diagram with efficient gain design based on a switch (SW) mode amplifier, as proposed in this work. **e**, Comparison of simulated total power transfer efficiency as a function of transfer distance achieved using the circuits in **c** and **d**. In **a**–**d**, P and Q are reference points where the gain element connects to the rest of the circuit. $k = k(d)$ denotes the coupling constant as a function of the transfer distance d.

of the source and receiver resonators, $\mathbf{a} = [a_s, a_r]^T$, is governed by $i\frac{d}{dt}\mathbf{a} = H(|a_s|)\mathbf{a}$ with the following nonlinear Hamiltonian[3]:

$$H(|a_s|) = \omega_0 \begin{bmatrix} 1 + i\frac{g(|a_s|)}{2} & \frac{k}{2} \\ \frac{k}{2} & 1 - i\frac{\gamma}{2} \end{bmatrix} \quad (1)$$

where ω_0 is the resonant frequency, k is the coupling constant between the two resonators (which varies with their separation distance) and g describes the strength of the gain in the source resonator. The gain saturates as $|a_s|$ increases. The detailed function form of $g(|a_s|)$ does not affect the transfer efficiency as long as the gain exhibits the saturation behaviour discussed above (see Supplementary Section 1 for further discussions). γ is the loss constant of the receiver resonator. If the unsaturated gain $g(|a_s|=0) > \gamma$ as time evolves, the system settles into a stable oscillating state due to gain saturation.

We can solve for these steady states by finding stable oscillatory states for the dynamics described by equation (1). Each state is characterized by its steady-state oscillation frequency ω_{ss} and its steady-state gain value g_{ss}. These parameters exhibit different characteristics depending on whether the system is in the strong coupling region ($k \geq \gamma$), which supports two steady states, or the weak coupling region ($k < \gamma$), which supports only one:

$$\omega_{ss} = \begin{cases} \omega_0, & k < \gamma \\ \omega_0\left[1 \pm \frac{1}{2}\sqrt{k^2 - \gamma^2}\right], & k \geq \gamma \end{cases} \quad (2)$$

and

$$g_{ss} = \begin{cases} k^2/\gamma, & k < \gamma \\ \gamma, & k \geq \gamma \end{cases} \quad (3)$$

In the strong coupling region, the system thus oscillates at a frequency that automatically adapts to the changing coupling rate. Moreover, such an oscillation frequency in fact corresponds to the frequency at which maximum transfer efficiency occurs in a standard wireless power transfer set-up[3]. Thus, in the nonlinear PT-symmetric wireless power transfer scheme, the transfer efficiency and delivered power are robust to transfer distance variations, without the need for any external tuning of the circuit. This is in contrast to the standard wireless power transfer scheme, which requires external tuning of the circuit to maintain high transfer efficiency as the transfer distance varies[12,29–31].

The original demonstration of the PT-symmetric wireless power transfer scheme achieves a high transfer efficiency, defined as the efficiency of the system to transfer power between the resonators. To achieve high system efficiency, however, it is also essential to optimize the efficiency of power injection into the system. Figure 1c presents a PT-symmetric wireless power transfer circuit similar to one used previously[3], which employs an operational-amplifier circuit to provide gain[32] to the source resonator. (This circuit has PT symmetry, even though the circuits on the source and receiver sides have different topology, as long as the quality factors of the resonances are sufficiently high[7].) Here, the voltage V_a across the resistor R_a feeds back into a differential-input linear voltage amplifier with voltage gain of two. Viewed from the source resonator, consisting of inductor L_1 and capacitor C_1, the combination of the amplifier and resistor R_a behaves like a resistor of value $-R_a$ (with the current direction opposite that of a normal resistor for a given applied voltage) that provides gain to the source resonator. However, because the current flows through the resistor R_a, there is a significant source of power loss at the resistor. As configured, for every unit of power flowing into the source resonator, an equal amount is lost through R_a, thus limiting the maximum efficiency to below 50%. The power-inefficient amplifier design used also limits the maximum system efficiency to below 30%. We also note that such an operational-amplifier circuit has been widely used as the gain element in recent studies on PT symmetry in radiofrequency circuits[3,33–35]. Thus, the issues of efficiency discussed here also limit the performance of all these PT-symmetric circuits.

High-efficiency gain design using a switch-mode amplifier

To improve the performance of the PT-symmetric wireless power transfer scheme, we developed a circuit design that uses a switch-mode

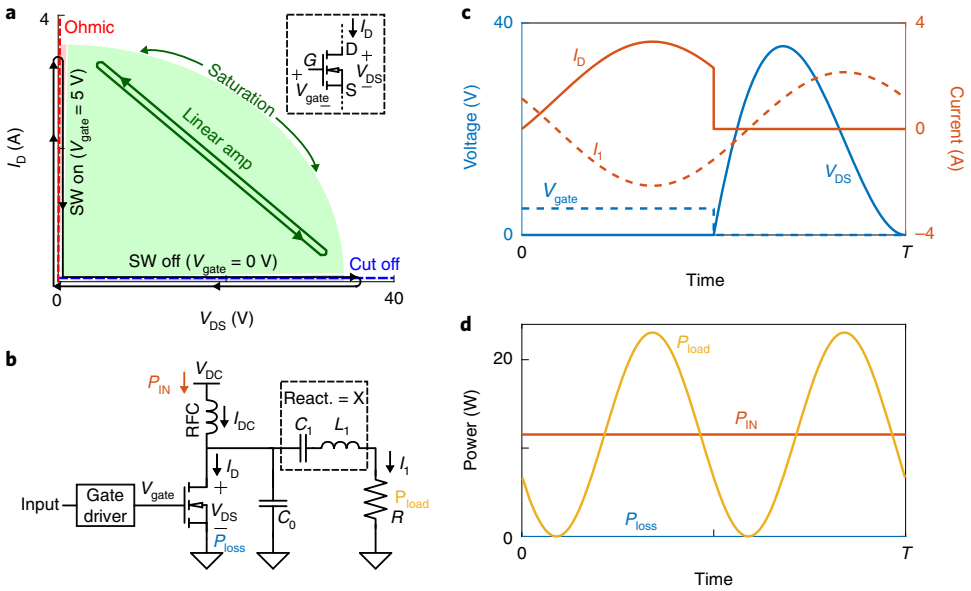

Fig. 2 | Power-efficient switch-mode amplifier operation. a, Parametric space between the drain-to-source voltage (V_{DS}) and drain current (I_D), showing the different transistor operating regimes (green shaded, saturation; red, ohmic; blue, cutoff) and representative traces used by a linear (green trace) and a switch-mode (black trace) amplifier design. **b**, A class E switch-mode amplifier circuit diagram. RFC, radiofrequency choke. **c**, Optimal waveforms of the transistor gate voltage (V_{gate}), drain-to-source voltage (V_{DS}), drain current (I_D) and load current (I_1). **d**, Waveforms of input power (P_{IN}), load power consumption (P_{load}) and transistor power loss (P_{loss}) for a switch-mode amplifier operating at its optimal efficiency condition. For this illustration, $V_{DS}=10$ V and $R=5\,\Omega$.

amplifier and current-sensing phase-delay feedback (Fig. 1d). This design achieves robust and efficient wireless power transfer with considerable improvement in efficiency compared to the previous approach (Fig. 1e). The switch-mode amplifier can be viewed as providing a nonlinear saturable negative resistance[6,7], similar to the operational-amplifier circuit, but without the associated intrinsic loss.

Transistors are a central part of electronic amplifiers, including the switch-mode amplifier. Specific operating regimes of the transistors are chosen via different designs of the amplifier, with important implications for the amplifier's linearity and power efficiency. Here we adopt MOSFET terminology for the terminal names and operating regimes, the latter being cutoff, ohmic and saturation (also called active)[36,37]. These different regimes of operation are labelled on the transistor's current–voltage plot in Fig. 2a. In a linear amplifier, the transistor is biased to operate in the saturation regime as a gate voltage-controlled current source—that is, a dependent source—where variations in input gate-to-source voltage (V_{gate}) produce offset and proportionally scaled variations in the transistor's drain current (I_D) and drain-to-source voltage (V_{DS}). The green curve in Fig. 2a depicts a representative trace of I_D and V_{DS} over one cycle for the linear amplifier. Here, the transistor spends a significant portion of a cycle with simultaneously high I_D and V_{DS}, resulting in wasted energy as a consequence of conduction loss in the transistor. The efficiency of the linear amplifier depends on the exact bias point and signal amplitude, but is typically below 80%[36,38]. Therefore, linear-amplifier designs are not favourable for efficiency-demanding applications.

In contrast, a switch-mode amplifier[36,38,39] can achieve near-unity efficiency by operating the transistor as a switch (black curve in Fig. 2a), alternating between switch on and switch off states, both of which have negligible conduction loss. Specifically, a large gate-to-source voltage (typically 5 V or higher) sets the transistor in the ohmic regime, which turns on drain-to-source conduction, corresponding to the switch-on state. A transistor specially designed to operate as a switch can have a very low on resistance on the order of milliohms in the ohmic regime. A low gate-to-source voltage (0 V) sets the transistor in the cutoff regime, which turns off drain-to-source conduction ($I_D=0$), corresponding to the switch-off state.

Figure 2b presents a switch-mode amplifier circuit in a configuration known as class E[38]. Here, the gate driver generates a square-wave signal V_{gate}, at switching frequency f, to control the transistor to be in the on- or off-switch state. The radiofrequency choke supplies the amplifier with constant current I_{DC}. The output filter L_1C_1 has small reactance $X=\omega L_1-1/\omega C_1$ at the switching frequency ($\omega=2\pi f$) and sufficiently high reactance at higher harmonics such that it constrains the line current I_1 flowing through the load R to be purely sinusoidal at ω. During the switch-off time, the current difference, $I_{DS}-I_1$, acts to charge capacitor C_0, leading voltage V_{DS} to develop in time. Over the switch-on duration, $V_{DS}=0$ and the current difference flows through the transistor as drain current instead. Although, here, only a negligible amount of energy is lost to conduction inside the transistor, the switch-mode operation may introduce switching loss. Suppose that, immediately before the switch-on time, voltage $V_{sw}=V_{DS}(t_{on}^-)$ across the output capacitor is not zero. As the switch is suddenly shorted, the energy in the capacitor will dissipate through the transistor, resulting in an energy loss of $1/2C_0V_{sw}^2$ per cycle. In Supplementary Section 2, the following efficient switching condition is established for 50% switch duty cycle as a relation between the switching frequency and the circuit parameters (ω, C_0, R, X) that results in $V_{SW}=0$, and therefore no switching loss:

$$\omega C_0 R = 0.184 \text{ and } \frac{X}{R} = 1.152 \quad (4)$$

Figure 2c shows the waveforms of I_D, I_1, V_{gate} and V_{DS} during one on/off cycle for a circuit satisfying the efficient switching condition. Voltage V_{DS}, which appears across C_0, indeed returns to zero immediately before the transistor is switched on for the following cycle. From Fig. 2d, which tracks the supplied power (P_{IN}), the transistor's power consumption (P_{loss}) and the power consumption at load R (P_{load}) during one cycle, we can see that the switch-mode amplifier is highly efficient, converting the supplied power to output power with virtually no loss.

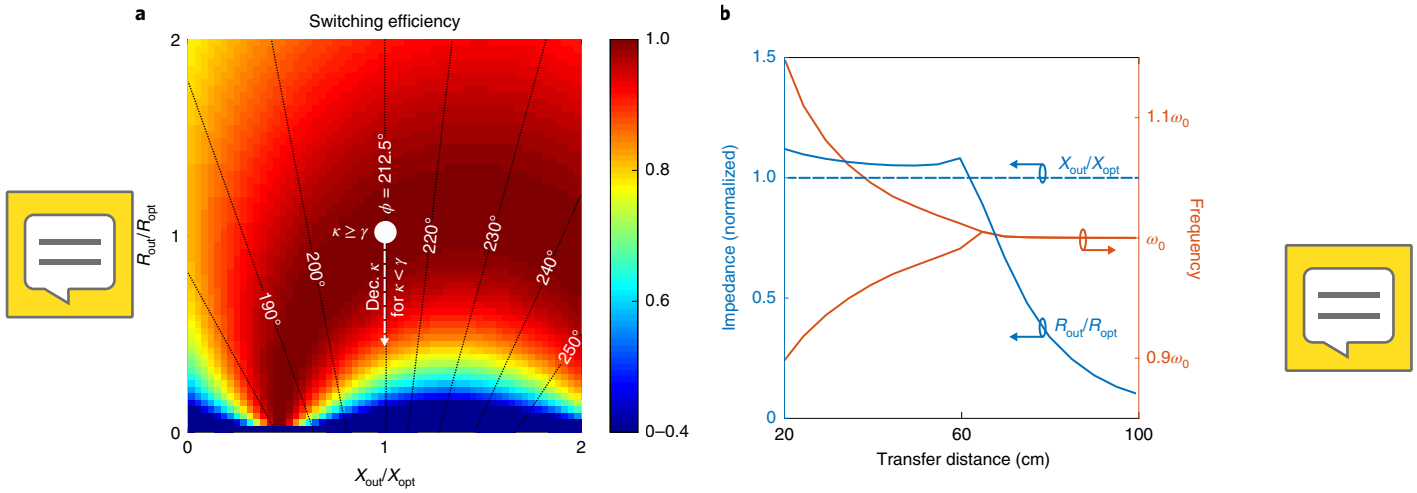

Fig. 3 | Efficient switch-mode amplifier as a resonator's gain element. a, Calculated switching efficiency as a function of the impedance being presented to the amplifier output ($Z_{out} = R_{out} + iX_{out}$), normalized to their respective optimal values ($R_{opt} = 0.184/\omega C_0$ and $X_{opt} = 1.154R_{opt}$) superimposed with contour lines showing the corresponding phase ϕ. The white dot indicates the operating point of the switch-mode amplifier in our circuit design in the strong coupling region, and the white dashed arrow represents movement of the operating point with decreasing coupling strength in the weak coupling region. **b**, Oscillation frequency and impedance values seen by the amplifier output as a function of the transfer distance calculated by fixing $\theta = 147.5°$ in our design (Fig. 1d). In the strong coupling region, the impedance values plotted correspond to the lower frequency branch.

Figure 3a presents the switching efficiency of the amplifier as a function of the real and imaginary parts of the total output impedance being presented to the amplifier ($Z_{out} = R_{out} + iX_{out}$) around their respective optimal values (R_{opt}, X_{opt} satisfying equation (4)) calculated using the model in Supplementary Section 2. The switching efficiency decreases as Z_{out} deviates away from the optimal condition of equation (4). When equation (4) is satisfied, the current I_1 flowing through Z_{out} has a phase delay of $\phi = 212.5°$ relative to the switch turn-on time, as shown in Fig. 3a, and can be observed from the respective waveforms in Fig. 2c.

When the switch-mode amplifier is introduced into the wireless power transfer system in Fig. 1d, the effective output impedance Z_{out} that the amplifier sees has contributions from the receiver's equivalent load, that is, $Z_{out} = \omega L_1 - \frac{1}{\omega C_1} + Z_{eq}(\omega, k)$, where $Z_{eq}(\omega,k)$ models the loading effect of the receiver on the source resonator. At a fixed ω, $Z_{eq}(\omega, k)$ depends on the coupling constant k. Thus, one might expect that the switch-mode amplifier may not be able to operate efficiently as the transfer distance varies. Remarkably, as long as the system has PT symmetry and is in the strong coupling region, the effective output impedance $Z_{out}(\omega_{ss})$ at the steady-state oscillation frequency ω_{ss}, which itself also varies as a function of the coupling constant, remains essentially independent of the coupling constant (as derived in detail in Supplementary Section 3). This effect arises because the variation of ω_{ss} on k works to cancel the direct effect of k in Z_{out}. The result here is in fact quite general: for an *LC* resonant circuit, its impedance at the resonant frequency is independent of the values of L and C. Therefore, a single choice of circuit parameters in equation (4) is sufficient to satisfy the efficient switching condition for the entire strong coupling region. Here, although we consider a class E amplifier as an example of a switch-mode amplifier, a similar effect exists when other types of switch-mode amplifier, such as half-bridge and full-bridge inverters, are used in PT-symmetric wireless power transfer circuits[6,7].

The appropriate switch input signal V_{gate} can be self-generated without an external control input by using phase-delay feedback. Taking into account the phase delay between the output current and the input signal as discussed above, we can use an opposite phase feedback delay of $\theta = 147.5°$ to generate the switch control signal and lock the amplifier in the efficient operating region. With this feedback in place, Fig. 3b shows that the effective impedance Z_{out} remains close to its optimal value throughout the strong coupling region, with the resistive part (R_{out}) decreasing with greater transfer distance in the weak coupling region. In the context of the parameter plot of Fig. 3a, the amplifier operating point stays near the optimal point (white dot) when the system is in the strong coupling region and moves down in the direction of lower R with decreasing k in the weak coupling region (dashed white line). The analysis above indicates that it is indeed possible to design a highly efficient PT-symmetric wireless power transfer system with the use of a switch-mode amplifier.

Based on the analysis above, we constructed a prototype, as shown in Fig. 4a. A pair of 58-cm-diameter copper coils form the inductive coupling link for wireless power transfer. The receiver's coil is configured as a parallel *RLC* resonator with 2.37 MHz resonant frequency ($\omega_0/2\pi$) and a measured quality factor ($1/\gamma$) of 29. The source coil ($L_1 = 8.9\,\mu H$) functions as the inductive element of the switch-mode amplifier's output filter. Capacitors $C_1 = 480\,pF$ and $C_0 = 2.2\,nF$ are selected to produce efficient switching according to the design procedure outlined above, taking into consideration the stray capacitances across the amplifier output and on the circuit board. The transistor switch is a gallium-nitride field-effect transistor type with very low on resistance (7 mΩ). The phase-delay feedback is implemented with a small coil in a weak inductive link to the source coil and produces a phase-delayed signal of the coil current to control the timing of the transistor through a gate driver. The phase feedback also functions as a starter: a brief start signal is applied here to overcome the threshold of the gate driver and start oscillations in the source resonator (see Methods).

We varied the separation distance d between the two coils from 20 cm to 100 cm (corresponding to a mutual coupling constant of $k = 0.253$–0.011). Figure 4b shows the oscillation frequency measurements, which exhibit the branching characteristic of the underlying eigenfrequencies of the PT-symmetric system (equation (2)). Power measurements were made at three locations: (1) the power intake at the amplifier ($P_{IN} \approx 10\,W$), (2) the extra power intake for the phase-delay feedback and gate driver, which represents an overhead consumption ($P_{aux} \approx 0.15\,W$) and remains relatively constant even when the amplifier supplied power is increased and (3) the

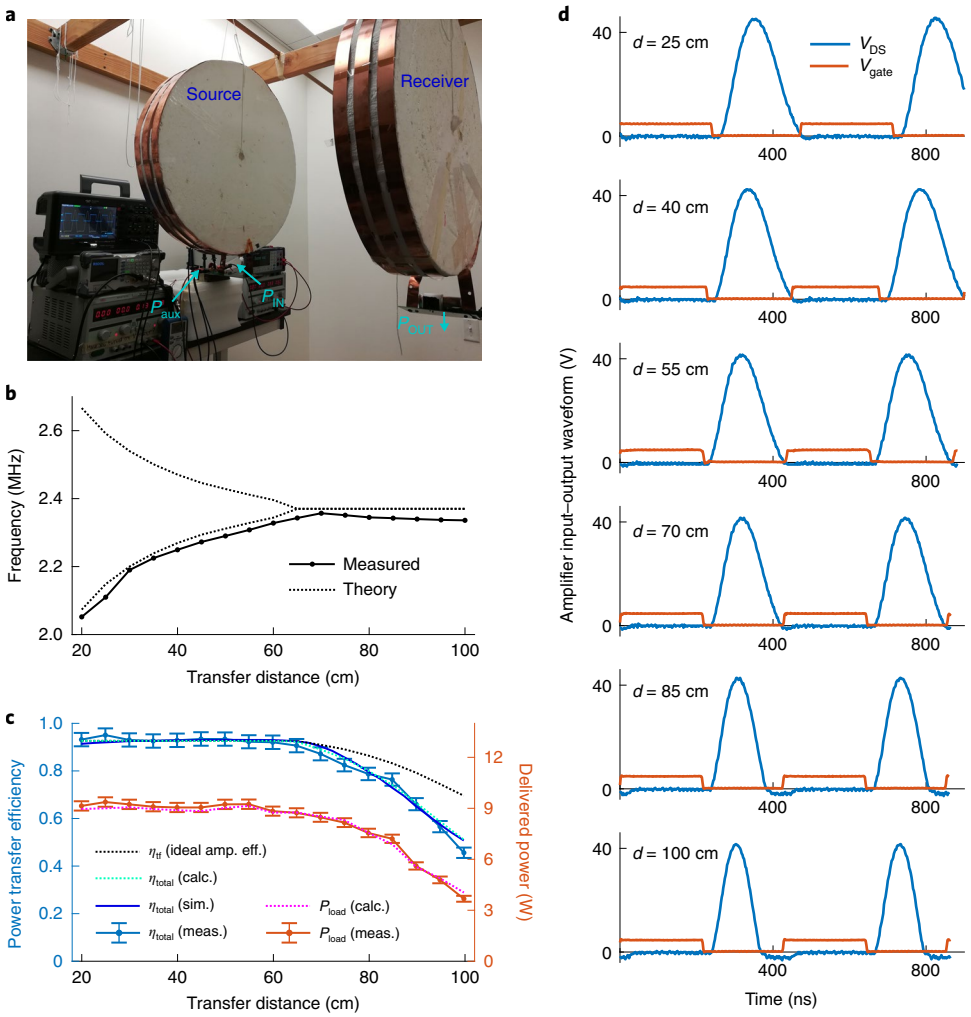

Fig. 4 | Experimental wireless power transfer system and measurements. a, Photograph of the experimental system. **b**,**c**, Oscillation frequency measurements (**b**) and delivered power efficiency simulation and measurements (**c**) as a function of transfer distance. **d**, Samples of the amplifier input (gate voltage) and output (drain-to-source voltage) waveforms recorded at various transfer distances. Error bars in **c** are 95% confidence limits.

delivered power at the receiver's load (P_{OUT}). Figure 4c shows the measured power transfer efficiency values in comparison with the theoretical and circuit simulation models as the transfer distance varies. The measured transfer efficiency is the total system efficiency, $\eta_{total} = P_{load}/(P_{IN} + P_{aux})$. The theoretical transfer efficiency, η_{tf}, is based on the ideal-amplifier model introduced in ref. [3], which only counts contributions from intrinsic losses inside the resonators and ignores losses inside the gain element. An almost flat 92% total efficiency is achieved for a transfer distance of up to 65 cm. This efficiency agrees with the prediction from the ideal-amplifier model, indicating that the switch-mode amplifier operates with almost no internal loss for a wide range of transfer distances in the strong coupling region. The total efficiency drops with larger transfer distance in the weak coupling region ($d > 65$ cm), more than the value obtained from the ideal-amplifier model, indicating that the switch-mode amplifier indeed departs from unity switching efficiency. Such a drop in the amplifier efficiency can be calculated by considering the switching and reverse conduction losses (Supplementary Section 4). These experimental observations agree with the theoretical analysis above. Figure 4d shows the input–output voltage waveforms of the switch-mode amplifier taken at various transfer distances. For a transfer distance of up to 65 cm, the amplifier output voltage (V_{DS}) returns to zero smoothly before the switch turn-on time, resulting in a highly power-efficient switching operation. At larger transfer distance, V_{DS} drops below zero and holds a small negative value (~ −2 V) until the start of the next cycle. When the transistor drain-to-source voltage reaches this level, the antiparallel diode turns on and automatically starts reverse conduction, which is responsible for the lowered efficiency. Here, we show that the efficiency is robust in the on-axis case, where only the distance between the source and the receiver varies. Similar robustness can be seen for misalignment between the source and receiver (Supplementary Fig. 1).

Conclusions

With our wireless power transfer system, which uses a switch-mode implementation of a nonlinear PT-symmetric circuit, we demonstrate a power transfer of around 10 W. This can be compared with previous experiments on PT-symmetric wireless power transfer schemes in which transferred power at a milliwatt level has been reported[3]. Further scaling up to a power level of multiple kilowatts should be possible, because transistors that can handle switching power greater than kilowatts are available[40,41]. Our work demonstrates that the concept of a wireless power transfer circuit based on nonlinear PT symmetry can be achieved with near-unity total power transfer efficiency. More generally, and in the context of the

emerging interest in PT-symmetric electronic circuits[26,33–35], our work indicates that the efficiency of such circuits can be systematically improved with the use of a switch-mode amplifier.

Methods

Coupled-mode model for resonant circuits. The coupled-mode parameters in equation (1) are related to the circuit parameters (Fig. 1a) as follows[34,42]: $\omega_0 = \frac{1}{\sqrt{L_2 C_2}}$ is the resonant frequency, $\gamma = \frac{\sqrt{L_2/C_2}}{R_2}$ is the loss (damping) factor for the parallel-connected receiver resonator and $g = \frac{|R_{neg}|}{\sqrt{L_1/C_1}}$ is the gain factor for the series-connected source resonator, where R_{neg} is the effective negative resistance of the gain element.

Circuit simulations used for power efficiency comparison. For the operational-amplifier-based circuit (Fig. 1c), the amplifier used for simulation was a Texas Instrument OPA548 high-power operational amplifier. The resonant frequencies were scaled down by a factor of 1,000 (L and C values scaled up by 1,000×) compared to the measurement set-up to be within the amplifier bandwidth. The operational amplifier was configured as a differential amplifier with a gain of 2. For the switch-mode design (Fig. 1d), the circuit parameters used were based on our measurement set-up. Supplementary Fig. 2 shows the full circuit diagrams used for total efficiency simulations.

Measurement set-up. The wireless power transfer circuit consisted of two units, the source and receiver. Two coils, each made of three turns of 2.54 cm × 0.25 mm copper ribbon rolled around a 58-cm-diameter foam core, with $L_1 = 8.9\,\mu H$ for the source and $L_2 = 9.0\,\mu H$ for the receiver, formed the basis of the wireless power transfer link. The two coils maintained coaxial alignment as the transfer distance between the two centres was varied. The receiver coil was connected in parallel to a pair of capacitors, one fixed (430 pF) and one tunable (5–85 pF), and to a model load consisting of a 4.0 kΩ power resistor in series with a 100 Ω precision resistor through which the delivered power was measured. A resonant frequency of 2.37 MHz and loaded quality factor of 29 were measured for the receiver resonator. The source coil was connected to the source circuit board containing the switch-mode amplifier and the phase-delay feedback circuitry to generate the switch signal. The amplifier design included a GS61008T transistor as a voltage-controlled switch, $C_0 = 2.2$ nF, $C_1 = 480$ F and a source coil for L_1. The amplifier was powered by a d.c. voltage power source through a 100 µH radiofrequency choke. The phase-delay feedback design, which generated a signal phase-shifted from the current I_1 through L_1, consisted of a 10-cm-diameter coil ($L_{fb} = 0.8\,\mu H$) weakly coupled ($k_{fb} = 0.01$) to L_1 in parallel with a variable resistor (set to 19 Ω). The variable resistor was set to effect near 147.5° total phase delay (from the current I_1 to the effective turn-on time of the switch). The actual phase delay was frequency-dependent, but the resulting phase variation with transfer distance was small (<5°), as shown in Supplementary Fig. 3. The phase compensation output was combined with a start signal and fed into an LT1711 comparator (with threshold and hysteresis set to ~10 mV) and then a LM5114 field-effect transistor gate driver to generate the switch signal. An arbitrary waveform generator (Rigol DG1062) generated a start signal (a burst of 10 cycles of a sine wave at 2.40 MHz and 5 V amplitude) to kickstart the oscillation. The transistor ran on a separate d.c. power supply set to output around 9–10 W of input power. All other components ran on a 5 V d.c. power supply with typical current draw of 30 mA. Digital multimeters took current measurements from each power supply line to arrive at the source circuit power intake. One oscilloscope monitored the amplifier's input and output voltage waveforms on the source unit, and another monitored the voltage waveform across the current-sense resistor on the receiver unit.

Data availability

The datasets generated and analysed during the current study are available at https://doi.org/10.6084/m9.figshare.11936229.v1.

Received: 16 September 2019; Accepted: 16 March 2020;
Published online: 20 April 2020

References

1. Kurs, A. et al. Wireless power transfer via strongly coupled magnetic resonances. *Science* **317**, 83–86 (2007).
2. Karalis, A., Joannopoulos, J. D. & Soljačić, M. Efficient wireless non-radiative mid-range energy transfer. *Ann. Phys.* **323**, 34–48 (2008).
3. Assawaworrarit, S., Yu, X. & Fan, S. Robust wireless power transfer using a nonlinear parity–time-symmetric circuit. *Nature* **546**, 387–390 (2017).
4. Chabalko, M. J., Shahmohammadi, M. & Sample, A. P. Quasistatic cavity resonance for ubiquitous wireless power transfer. *PLoS ONE* **12**, e0169045 (2017).
5. Ra'Di, Y. et al. On-site wireless power generation. *IEEE Trans. Antennas Propag.* **66**, 4260–4268 (2018).
6. Hou, Y., Lin, M., Chen, W. & Yang, X. Parity–time-symmetric wireless power transfer system using switch-mode nonlinear gain element. In *2018 IEEE International Power Electronics and Application Conference and Exposition (PEAC)* 1–5 (IEEE, 2018); https://doi.org/10.1109/PEAC.2018.8590364
7. Zhou, J., Zhang, B., Xiao, W., Qiu, D. & Chen, Y. Nonlinear parity–time-symmetric model for constant efficiency wireless power transfer: application to a drone-in-flight wireless charging platform. *IEEE Trans. Ind. Electron.* **66**, 4097–4107 (2019).
8. Donaldson, P. E. K. Power for neurological prostheses: a simple inductive RF link with improved performance. *J. Biomed. Eng.* **9**, 194–197 (1987).
9. Donaldson, P. E. K. Three separation-insensitive radiofrequency inductive links. *J. Med. Eng. Technol.* **11**, 23–29 (1987).
10. Zierhofer, C. M. & Hochmair, E. S. High-efficiency coupling-insensitive transcutaneous power and data transmission via an inductive link. *IEEE Trans. Biomed. Eng.* **37**, 716–722 (1990).
11. Kurs, A., Moffatt, R. & Soljačić, M. Simultaneous mid-range power transfer to multiple devices. *Appl. Phys. Lett.* **96**, 044102 (2010).
12. Sample, A. P., Meyer, D. A. & Smith, J. R. Analysis, experimental results and range adaptation of magnetically coupled resonators for wireless power transfer. *IEEE Trans. Ind. Electron.* **58**, 544–554 (2011).
13. Yu, X., Sandhu, S., Beiker, S., Sassoon, R. & Fan, S. Wireless energy transfer with the presence of metallic planes. *Appl. Phys. Lett.* **99**, 214102 (2011).
14. Yu, X. et al. Wireless power transfer in the presence of metallic plates: experimental results. *AIP Adv.* **3**, 062102 (2013).
15. Ho, J. S. et al. Wireless power transfer to deep-tissue microimplants. *Proc. Natl Acad. Sci. USA* **111**, 7974–7979 (2014).
16. Hui, S. Y. R., Zhong, W. & Lee, C. K. A critical review of recent progress in mid-range wireless power transfer. *IEEE Trans. Power Electron.* **29**, 4500–4511 (2014).
17. Li, S. & Mi, C. C. Wireless power transfer for electric vehicle applications. *IEEE J. Emerg. Sel. Top. Power Electron.* **3**, 4–17 (2015).
18. Wang, G., Liu, W., Sivaprakasam, M. & Kendir, G. A. Design and analysis of an adaptive transcutaneous power telemetry for biomedical implants. *IEEE Trans. Circuits Syst. I* **2**, 2109–2117 (2005).
19. Brecher, A. & Arthur, D. *Review and Evaluation of Wireless Power Transfer (WPT) for Electric Transit Applications* Report No. 0060 (FTA, 2014).
20. Rüter, C. E. et al. Observation of parity–time symmetry in optics. *Nat. Phys.* **6**, 192–195 (2010).
21. El-Ganainy, R. et al. Non-Hermitian physics and PT symmetry. *Nat. Phys.* **14**, 11–19 (2018).
22. Feng, L., Wong, Z. J., Ma, R.-M., Wang, Y. & Zhang, X. Single-mode laser by parity-time symmetry breaking. *Science* **346**, 972–975 (2014).
23. Guo, A. et al. Observation of PT-symmetry breaking in complex optical potentials. *Phys. Rev. Lett.* **103**, 093902 (2009).
24. Lin, Z. et al. Unidirectional invisibility induced by PT-symmetric periodic structures. *Phys. Rev. Lett.* **106**, 213901 (2011).
25. Doppler, J. et al. Dynamically encircling an exceptional point for asymmetric mode switching. *Nature* **537**, 76–79 (2016).
26. Chen, P.-Y. et al. Generalized parity–time symmetry condition for enhanced sensor telemetry. *Nat. Electron.* **1**, 297–304 (2018).
27. Chen, W., Kaya Özdemir, Ş., Zhao, G., Wiersig, J. & Yang, L. Exceptional points enhance sensing in an optical microcavity. *Nature* **548**, 192–196 (2017).
28. Hodaei, H. et al. Enhanced sensitivity at higher-order exceptional points. *Nature* **548**, 187–191 (2017).
29. Sample, A. P., Waters, B. H., Wisdom, S. T. & Smith, J. R. Enabling seamless wireless power delivery in dynamic environments. *Proc. IEEE* **101**, 1343–1358 (2013).
30. Kim, N. Y., Kim, K. Y., Choi, J. & Kim, C.-W. Adaptive frequency with power-level tracking system for efficient magnetic resonance wireless power transfer. *Electron. Lett.* **48**, 452–454 (2012).
31. Beh, T. C., Kato, M., Imura, T., Oh, S. & Hori, Y. Automated impedance matching system for robust wireless power transfer via magnetic resonance coupling. *IEEE Trans. Ind. Electron.* **60**, 3689–3698 (2013).
32. Larky, A. Negative-impedance converters. *IRE Trans. Circuit Theory* **4**, 124–131 (1957).
33. Schindler, J., Li, A., Zheng, M. C., Ellis, F. M. & Kottos, T. Experimental study of active LRC circuits with PT symmetries. *Phys. Rev. A* **84**, 040101 (2011).
34. Schindler, J. et al. PT-symmetric electronics. *J. Phys. A* **45**, 444029 (2012).
35. Lin, Z., Schindler, J., Ellis, F. M. & Kottos, T. Experimental observation of the dual behavior of PT-symmetric scattering. *Phys. Rev. A* **85**, 050101 (2012).
36. Kazimierczuk, M. K. *RF Power Amplifiers* (Wiley, 2008).
37. Sedra, A. S. & Smith, K. C. *Microelectronic Circuits* (Oxford Univ. Press, 2010).
38. Raab, F. Idealized operation of the class E tuned power amplifier. *IEEE Trans. Circuits Syst.* **24**, 725–735 (1977).
39. Raab, F. H. et al. Power amplifiers and transmitters for RF and microwave. *IEEE Trans. Microw. Theory Tech.* **50**, 814–826 (2002).
40. Li, H. et al. Design of a 10 kW GaN-based high power density three-phase inverter. In *2016 IEEE Energy Conversion Congress and Exposition (ECCE)* 1–8 (IEEE, 2016); https://doi.org/10.1109/ECCE.2016.7855019

41. Choi, J., Tsukiyama, D., Tsuruda, Y. & Davila, J. M. R. High-frequency, high-power resonant inverter with eGaN FET for wireless power transfer. *IEEE Trans. Power Electron.* **33**, 1890–1896 (2018).
42. Haus, H. A. *Waves and Fields in Optoelectronics* (Prentice Hall, 1984).

Acknowledgements

This work was supported by a Vannevar Bush Faculty Fellowship (grant no. N00014-17-1-3030) from the US Department of Defense.

Author contributions

S.A. performed the simulations and measurements. S.F. supervised the project. Both authors contributed to writing the manuscript.

Competing interests

The authors declare no competing interests.

Additional information

Supplementary information is available for this paper at https://doi.org/10.1038/s41928-020-0399-7.

Correspondence and requests for materials should be addressed to S.F.

Reprints and permissions information is available at www.nature.com/reprints.

Publisher's note Springer Nature remains neutral with regard to jurisdictional claims in published maps and institutional affiliations.